ISSN: 2278-4632
Vol-10 Issue-09 No.03 September 2020

# Numerical Study of Flow Modification Techniqueto Mitigate Wave Drag by Counterflow Supersonic Jet in Hypersonic Flow

[1]BHABANI SANKAR SI,

*Gandhi Institute of Excellent Technocrats, Bhubaneswar, India*

[2]UMAKANTA PUTHAL,

*Kruttika Institute of Technical Education, Khordha, Odisha, India*

***Abstract:*** Reducing aerodynamic wave drag is critically essential in any successful space mission. A computational study to mitigation of wave drag by supersonic counterflow jet in hypersonic flow has been performed using in-house solver. In this research paper, an axisymmetric Euler equation is used as governing equation. Study has been carried out for an axisymmetric $60^0$ apex-angle blunt nose with and without opposing jet since Mach number of flow are 8.0. The discretization based upon Finite Volume Method (FVM). Here Van Leer Flux Splitting Scheme will be used for capturing convective fluxes. Species continuity equations are also incorporated with the Euler solver. The computational result shows up to 39% reduction in wave drag coefficient under opposing supersonic jet.

***Keywords:*** Flow modification Technique, opposing jet, wave drag, FVM.

## I. INTRODUCTION

To achieve every space mission, one has to go through hypersonic speed. One has to achieve hypersonic speed while entering space or re-entering the earth. Hypersonic wave drag and surface heating have been major problems at this speed. Therefore, to complete any space mission or hypersonic flight securely and successfully, it is necessary to reduce it. One of the most well-known examples of the repercussions of aerodynamic heating is the Columbia Space Shuttle's disaster during re-entry to earth in 2003 [1]. The physical cause of the loss of Columbia and its crew was a breach in the thermal protection System (TPS) on the leading edge of the left wing. External heat enters into the space shuttle leads to complete destruction of the space craft. Many techniques have been investigated in the past by many researchers, out of which these three methods are very effective for working the drag and heat. These are energy deposition in the upstream of nose, aerospike/aero disk at nose stagnation point and counterflow supersonic jet which emanating from stagnation point of the nose. All these techniques are flow modification technique. All these methods are flow modifiers techniques in which the wave drag and surface heat are reduced by modifying the flow field around the nose of the vehicle. In this counter flow opposing jet is very effective to reduce wave drag as well as surface heat. In recent years, there has been a lot of interest in deploying a forward-facing supersonic jet that emerges from a blunt body's stagnation point to reduce wave drag and heat flux when flying at hypersonic Mach numbers. Nair et al. [2], Zheng et al. [3] Yisheng [4] investigated the wave drag and thermal load reduction by counter-flowing jets through numerical analysis and testing. The effect of the nozzle pressure ratio on the decrease in aerodynamic heating was explored. The heat flux at each location reduced as the pressure ratio increased, according to their experiment and numerical simulation results [5]. The study on ANSYS is suitability as a CFD tool, which could be useful to a designer of hypersonic vehicle. However, the impact of injecting a continuous jet, which causes significant oscillation in the flow field around the frontal portion of the bluff body, could indicate instability, implying thermal oscillation and heat dispersion comparable to vortex shedding [6]. Sharma and Nair [7] quantitatively investigated different nose-tips with opposing jets for supersonic speed and hypersonic speed free stream conditions. Their findings revealed a direct link between the nose's configuration and the opposing jet's thermal protection impact. The surface heat flux distributions in [8] experiment using nitrogen gas as the counterflowing cooling jet have been often used as the verification case for numerical simulation by researcher [9],[10] including the authors themselves. Only pressure ratios greater than 0.2 were evaluated for steady flow in their research since unstable gas injection had the opposite impact in the thermal protection experiment. Xie et al. [11] and Shen et al. [12] investigated the numerical properties of spherical and blunt nose in supersonic and hypersonic freestreams. To forecasting the flow field around the body, the researcher employed the Static Pressure Ratio (SPR) of the jet and freestream rather of the overall SPR. Li et al. [13] investigated the porous jet design is effective in increasing the overall performance of the blunt hypersonic vehicle by reducing drag and providing thermal shielding. Because the porous jet has a three-dimensional effect, an ideal injection


Copyright @ 2020 Authors

ISSN: 2278-4632
Vol-10 Issue-09 No.03 September 2020

technique exists. Venukumar et al. [14] investigated the drag on the nose at hypersonic speeds could be reduced by up to 66 percent if the counterflowing jet generates reverse thrust. The model's highest lift-to-drag ratio is attained at 6°, while the counterflowing jet reduces drag by 8.8 percent throughout the entire model. A counterflowing opposing jet's drag reduction for a 60-degree apex angle bluff nose is also numerically investigated using CFD. Figure 1 shows a schematic illustration of the flow field features around the blunt cone with a counterflowing jet. A counterflowing supersonic jet's drag reduction for a 60-degree apex angle blunt cone is also numerically investigated using CFD. Figure 1 shows a schematic illustration of the flow field features around the blunt cone with a counterflowing jet.

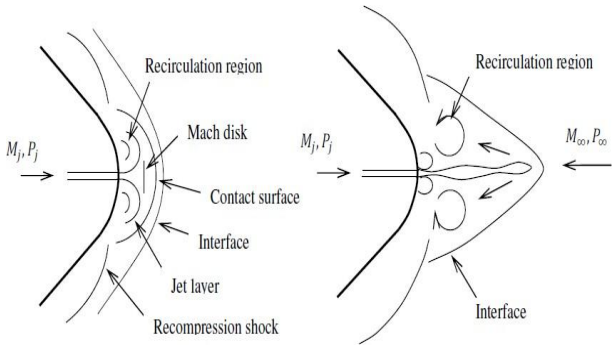


**Figure 1:** Flow field around blunt nose due to counter jet

## II. NUMERICAL METHODOLOGY

The Euler equation [15] is the governing equation. The conservation of mass, momentum, energy and species continuity are essentially expressed by the Euler equation. These can be written in two-dimensional Cartesian coordinates as

$$\frac{\partial \vec{U}_i}{\partial t} + \frac{\partial \vec{F}_i}{\partial x} + \frac{\partial \vec{G}_i}{\partial y} = 0 \qquad (1)$$

$$\vec{U}_i = \begin{bmatrix} \rho \\ \rho u \\ \rho v \\ \rho E \\ \rho m \end{bmatrix}_i \quad \vec{F}_i = \begin{bmatrix} \rho u \\ \rho u^2 + p \\ \rho uv \\ \rho uH \\ \rho um \end{bmatrix}_i \quad \vec{G}_i = \begin{bmatrix} \rho u \\ \rho uv \\ \rho v^2 + p \\ \rho uH \\ \rho vm \end{bmatrix}_i$$

The Euler equations regulating 2D flow in the absence of body forces in the conservative and differential versions are,

$$\frac{\partial(\rho)}{\partial t} + \frac{\partial(\rho u)}{\partial x} + \frac{\partial(\rho v)}{\partial y} = 0 \qquad (2)$$


Copyright @ 2020 Authors

ISSN: 2278-4632
Vol-10 Issue-09 No.03 September 2020

$$\frac{\partial(\rho u)}{\partial t}+\frac{\partial(\rho u^2+p)}{\partial x}+\frac{\partial(\rho v)}{\partial y}=0 \quad (3)$$

$$\frac{\partial(\rho E)}{\partial t}+\frac{\partial(\rho u H)}{\partial x}+\frac{\partial(\rho v H)}{\partial y}=0 \quad (4)$$

$$\frac{\partial(\rho m_i)}{\partial t}+\frac{\partial(\rho u m_i)}{\partial x}+\frac{\partial(\rho v m_i)}{\partial y}=0 \quad (5)$$

The total specific energy, E=e+0.5(u2+v2), and the total specific enthalpy, H=h+0.5(u2+v2), are the mass fraction of the species indicated by mi=i / in the previous formulations. The perfect gas relations can be used in conjunction with the effective thermodynamic properties for gas mixtures, or the perfect gas relations can be used in conjunction with the effective thermodynamic properties for gas mixtures.

$$R=\sum M_i R_i \quad \gamma=\sum M_i \gamma_i$$

For the 2-D axi-symmetric problems the finite volume formulation is given by

$$\frac{dU}{dt}+\frac{1}{V}\oint_{S(t)} \vec{n}.\vec{F}ds=S \quad \text{, here} \quad S=-\frac{1}{r}\begin{bmatrix}\rho v\\ \rho uv\\ \rho v^2\\ (e+p)v\end{bmatrix}$$

$\overline{U}$ is the average value of $U$ over the entire control volume, $F$ is the flux vector and $n$ is the unit normal to the surface. And $F=F_I i+G_I j$ , is the total inviscid flux, upon integrating the inviscid flux over the faces of k[th] control volume the above equation becomes

$$\frac{\partial U_k}{\partial t}+\frac{1}{V_k}\left[\sum_{i=1}^{nf}\vec{F}.\vec{n}ds\right]_k=0 \quad (6)$$

Here, $\vec{n}=\frac{\Delta y_i}{\Delta s^i}\vec{i}-\frac{\Delta x_i}{\Delta s^i}\vec{j}$ and $\Delta s_i=\sqrt{(\Delta x)_i^2+(\Delta y)_i^2}$

The wave drag coefficient, a non-dimensional metric defined by, is used to estimate net drag.

$$C_d=\frac{2F_d}{\rho_\infty V_\infty^2 A}=\frac{1}{\rho_\infty V_\infty^2 A}\int_s (P-P_\infty).\vec{n}.dA \quad (7)$$

Jet pressure ratio ($P_j$) is defined as by equation (8),

$$P_j=\frac{P_{oj}}{P_{0\infty}} \quad (8)$$

where $P_{oj}$ is total jet pressure and $P_{0\infty}$total freestream pressure.

**Geometry and Grid**

Figure 2 shows a typical grid for calculating flow fields around a $60^0$ Apex-angle blunt body model is taken from reference [8] with a 2 mm jet diameter in the nose area.


Copyright @ 2020 Authors

ISSN: 2278-4632
Vol-10 Issue-09 No.03 September 2020

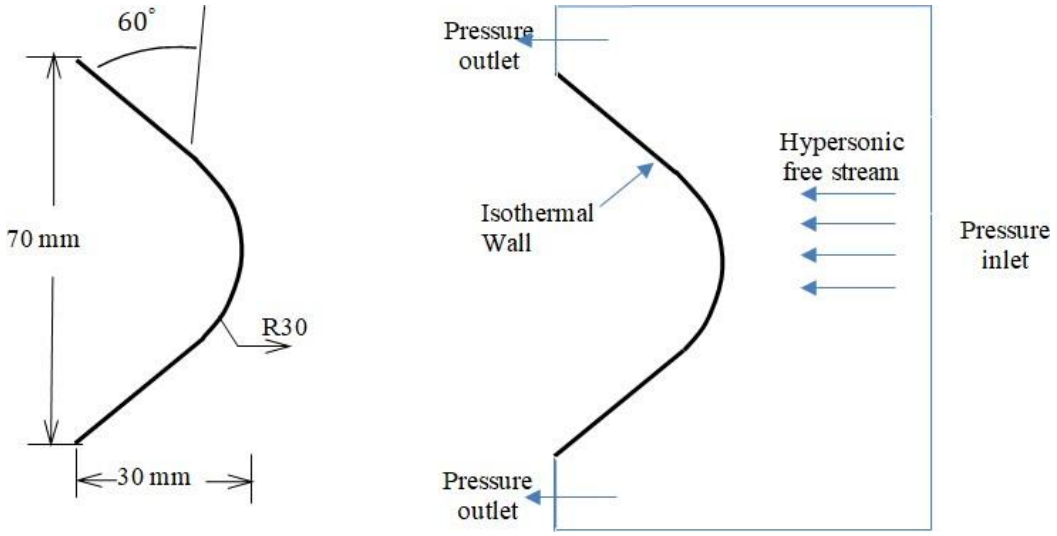


**Figure 2:** $60^0$ Bluff Body and 2mm nozzle at stagnation point [14]

For present situation angle of attack for flow is zero hence for reducing computational time half part is consider for analysis. Figure 3 shows the grid system used in the present study. In the x-direction (along the body), there are 205 grid points and 150 in the y-direction (perpendicular to the body).

**Boundary conditions**

2D solid boundary fluxes, Inviscid or slip wall boundary condition, Pressure extrapolation boundary condition, Mirror image boundary condition, and Far field boundary condition are all frequent boundary conditions for two-dimensional inviscid flow problems.

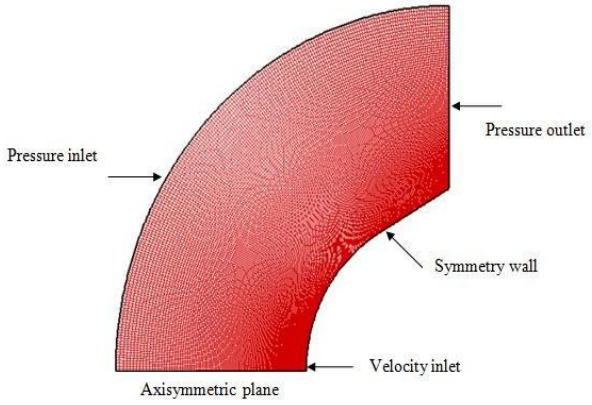


**Figure 3:** Grid Boundary conditions and (205×150)

**Table 1:** Free stream condition for flow

| Fluid | Static pressure (Pa) | Static temperature (K) | Mach number | Velocity (m/s) |
|---|---|---|---|---|
| Air | 284.0 | 316.0 | 8.0 | 2850.62 |


Copyright @ 2020 Authors

ISSN: 2278-4632
Vol-10 Issue-09 No.03 September 2020

**Table 2:** Flow condition for opposing counter jet: Air as injecting gas

| Gas | Total pressure (bar) | Total Temperature (K) | Mach number |
|---|---|---|---|
| Air | 2.0 | 300.0 | 1.0 |
| | 4.0 | 300.0 | 1.0 |
| | 6.0 | 300.0 | 1.0 |
| | 8.0 | 300.0 | 1.0 |

**Solver Validation**

The flow solver is validated for Mach number (M=8) in order to forecast the fluctuation of shock stand-off distance with Mach number. The solver's shock detachment distance was compared to the Billig correlation for shock detachment distance, which is provided by for cylinder,

$$\frac{\delta}{R} = 0.386\exp\left(\frac{4.67}{M^2_\infty}\right), \quad \frac{R_c}{R} = 1.386\exp\left(\frac{1.8}{(M_\infty - 1)^{0.75}}\right) \tag{9}$$

The research is subsequently expanded to predict the shock wave shape from the solver, which is supported by empirical data.

$$x = R + \delta - R_c \cot^2\beta\left[\left(1 + \frac{y^2\tan^2\beta}{R_c}\right)^{1/2} - 1\right] \tag{10}$$

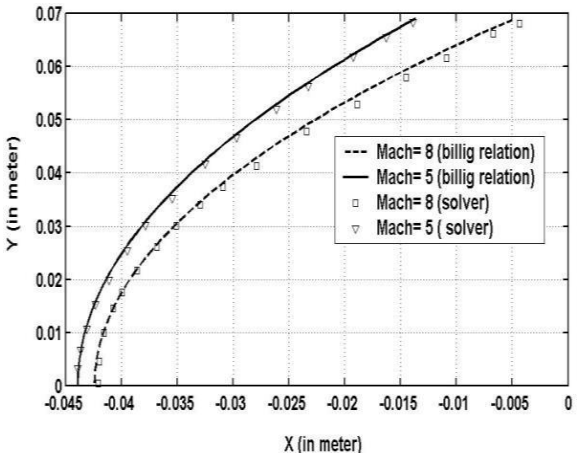


**Figure 4:** Comparison of shock shape with empirical correlation

**III. RESULT**

The numerical results for drag force computations with supersonic jet injection are obtained using the procedures described in the previous sections for four different injection pressure ratios, namely 7.45, 14.91, 22.36, and 29.82, which correspond to 2, 4, 6, and 8 bar jet stagnation pressures, respectively. The numerical results result in a variety of outputs. The current study's main findings include the effects of total pressure ratio, graphical representation, and contour representations. Figure 6 shows that a powerful bow shock wave develops at the nose region, reducing the body's speed. This increases the amount of drag in the nose area.


Copyright @ 2020 Authors

ISSN: 2278-4632
Vol-10 Issue-09 No.03 September 2020

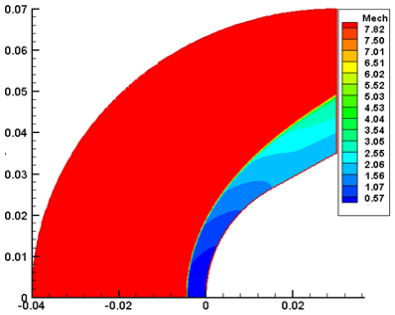


**Figure 6:** Mach contour without supersonic counter jet

**Table 3:** Drag coefficient for different jet injection pressures (with air as injecting gas)

| Injection pressure (bar) | Coefficient of drag ($C_d$) | Reduction in $C_d$ (%) |
|---|---|---|
| 0 | 0.8717 | ----- |
| 2.0 | 0.7567 | 13.2% |
| 4.0 | 0.6506 | 25.4% |
| 6.0 | 0.5875 | 32.6% |
| 8.0 | 0.5322 | 38.9% |

Table 3 shows the coefficient of drag on the cone's surface with and without a counter jet. The reduction in wave drag clearly seen from the table. Figure 7 shows the Mach number contours to show the real amount of drag on the body in the presence of a jet. For total pressure ratios, the Mach curve is used.

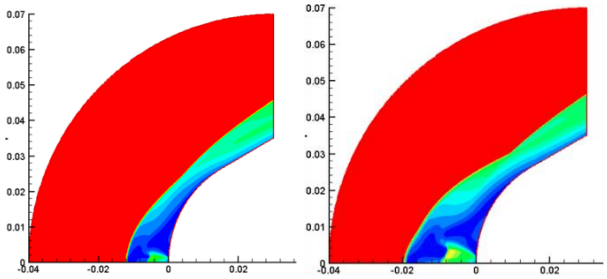


"(a)" P=7.45 " (b)" P=14.91

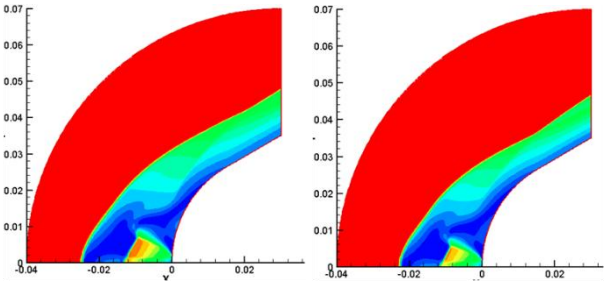


"(c)" P=22.36 "(d)" P=29.82

**Figure 7:** Mach number contour at different pressure jet ratio


Copyright @ 2020 Authors

ISSN: 2278-4632
Vol-10 Issue-09 No.03 September 2020

Here is a graphical representation of pressure drag and static pressure distribution for the blunt body that illustrates the comparison study between the case in the absence of jet and the case in the presence of jet. Figure 8 shows a comparison of static pressure distribution in the absence of a jet and in the presence of a jet under various jet settings. In the case of no injection, a significant amount of static pressure distribution can be detected at the nose region. In the injection instance, analysis of the static pressure distribution reveals that the nasal static pressure distribution is lowest at the tip and subsequently increases somewhat due to the recompression shock wave.

**Table 4:** Surface pressure from stagnation point of the nose

| | Wall Pressure (kPa) | | | | |
|---|---|---|---|---|---|
| Theta (Degree) | Pr=0 | Pr=7.45 | Pr=14.91 | Pr=22.36 | Pr=29.82 |
| 0 | 17.80 | 5.73 | 5.00 | 5.00 | 3.80 |
| 6 | 16.67 | 5.40 | 4.47 | 4.47 | 3.74 |
| 12 | 15.21 | 4.54 | 3.87 | 3.87 | 3.20 |
| 18 | 13.62 | 4.08 | 3.54 | 3.54 | 2.54 |
| 24 | 11.96 | 4.41 | 4.48 | 4.48 | 2.34 |
| 30 | 10.70 | 5.22 | 5.22 | 5.22 | 2.55 |
| 36 | 9.24 | 6.22 | 6.03 | 6.03 | 3.15 |
| 42 | 7.59 | 7.17 | 6.90 | 6.90 | 4.56 |
| 48 | 6.00 | 7.84 | 6.97 | 6.97 | 5.10 |
| 54 | 4.94 | 8.44 | 6.78 | 6.78 | 5.31 |
| 60 | 4.69 | 8.85 | 6.32 | 6.32 | 4.92 |
| 66 | 4.50 | 8.86 | 5.14 | 5.14 | 4.33 |
| 72 | 4.58 | 8.53 | 5.02 | 5.02 | 3.74 |
| 78 | 4.66 | 7.94 | 4.90 | 4.90 | 3.75 |
| 84 | 4.73 | 7.28 | 4.78 | 4.78 | 3.77 |
| 90 | 4.73 | 7.27 | 4.77 | 4.77 | 3.76 |

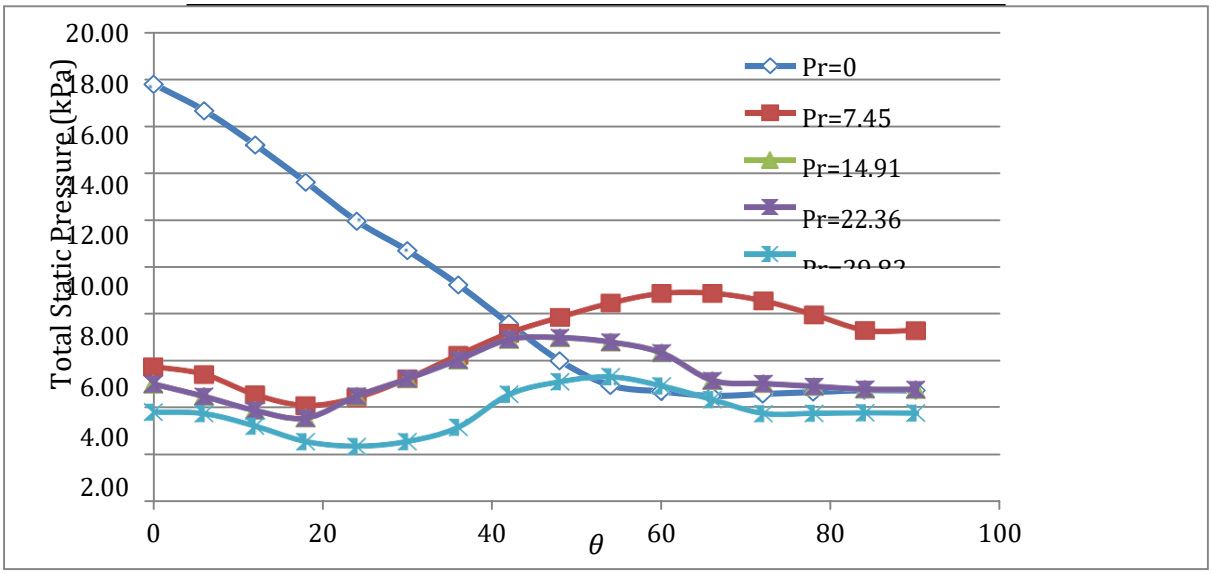


**Figure 8:** Static pressure distribution with and without counter jet


Copyright @ 2020 Authors

ISSN: 2278-4632
Vol-10 Issue-09 No.03 September 2020

## IV. CONCLUSION

CFD is used to explore drag reduction in hypersonic flow with counterflow jet in this work. The dimensional axisymmetric Euler equation is used to determine the detailed flow field with counterflow jet in hypersonic flow. Empirical correlations are used to validate the solver and numerical results. When the opposing jet flows, there is a significant reduction in drag. For various jet pressures, the numerical result reveals a reduction in drag coefficient of 38.9 percent. It becomes evident that the performance of an opposing jet in reducing aerodynamic wave drag is highly influenced by jet condition.

## REFERENCES

[1] "NASA - Report of Columbia Accident Investigation Board, Volume I", *Nasa.gov*, 2022. [Online]. Available: https://www.nasa.gov/columbia/home/CAIB_Vol1.html. [Accessed: 06- May- 2022].

[2] Y. Zheng, N. Ahmed and W. Zhang, "Heat Dissipation using Minimum Counter Flow Jet Ejection During Spacecraft Re-Entry", *Procedia Engineering*, vol. 49, pp. 271-279, 2012. Available: 10.1016/j.proeng.2012.10.137 [Accessed 6 May 2022].

[3] P. Nair, T. Jayachandranl, M. Deepu, B.P. Puranik and U.V. Bhandarkar, "Numerical Simulation of Interaction of Sonic Jet with High Speed Flow over a Blunt Body using Solution Mapped Higher Order Accurate AUSM+-UP Based Flow Solver", *Journal of Applied Fluid Mechanics*, vol. 3, no. 01, 2010. Available: 10.36884/jafm.3.01.11875.

[4] R. Yisheng, "Drag reduction research in supersonic flow with opposing jet", *Acta Astronautica*, vol. 91, pp.1-7, 2013. Available: 10.1016/j.actaastro.2013.04.015 [Accessed 6 May 2022].

[5] K. Hayashi, S. Aso and Y. Tani, "Numerical Study of Thermal Protection System by Opposing Jet", 43rd AIAA Aerospace Sciences Meeting and Exhibit, 2005. Available: 10.2514/6.2005-188 [Accessed 7 May 2022].

[6] Y. Zheng, N. A. Ahmed, and W. Zhang, "Heat dissipation using minimum counter flow jet ejection during spacecraft re-entry," Procedia Engineering, vol. 49, pp. 271–279, 2012. Available: 10.1016/j.proeng.2012.10.137

[7] K. Sharma and M. Nair, "Combination of counterflow jet and cavity for heat flux and drag reduction", Physics of Fluids, vol. 32, no. 5, p. 056107, 2020. Available: 10.1063/1.5143521 [Accessed 7May 2022].

[8] K. Hayashi, S. Aso and Y. Tani, "Experimental Study on Thermal Protection System by Opposing Jet in Supersonic Flow", *Journal of Spacecraft and Rockets*, vol. 43, no. 1, pp. 233-235, 2006. Available: 10.2514/1.15332.

[9] W. Huang, Y. Jiang, L. Yan and J. Liu, "Heat flux reduction mechanism induced by a combinational opposing jet and cavity concept in supersonic flows", *Acta Astronautica*, vol. 121, pp. 164-171, 2016. Available: 10.1016/j.actaastro.2016.01.008.

[10] W. Huang, L. Yan, J. Liu, L. Jin and J. Tan, "Drag and heat reduction mechanism in the combinational opposing jet and acoustic cavity concept for hypersonic vehicles", *Aerospace Science and Technology*, vol.42, pp. 407-414, 2015. Available: 10.1016/j.ast.2015.01.029.

[11] W. XIE, Z. LUO, Y. ZHOU, W. PENG, Q. LIU and D. WANG, "Experimental and numerical investigation on opposing plasma synthetic jet for drag reduction", Chinese Journal of Aeronautics, 2021.Available: 10.1016/j.cja.2021.10.027.

[12] B. Shen, W. Liu and L. Yin, "Drag and heat reduction efficiency research on opposing jet in supersonic flows", Aerospace Science and Technology, vol. 77, pp. 696-703, 2018. Available: 10.1016/j.ast.2018.03.051.

[13] S. Li, W. Huang, Z. Wang and L. Yan, "Drag and Heat Reduction Mechanism of the Porous Opposing Jet for Variable Blunt Hypersonic Vehicles", Volume 5B: Heat Transfer, 2018. Available: 10.1115/gt2018- 75151 [Accessed 7 May 2022].

[14] B. Venukumar, G. Jagadeesh, and K. P. Reddy, "Counterflow drag reduction by supersonic jet for a bluntbody in hypersonic flow," *Physics of Fluids*, vol. 18, no. 11, p. 118104, 2006.

[15] Anderson, J. D. (1989). Hypersonic and High Temperature Gas Dynamics. McGraw-Hill Inc.


Copyright @ 2020 Authors